Alumina feeding and raft formation: Raft collection and process parameters

Sindre Engzelius Gylver, Nina Helene Omdahl, Ann Kristin Prytz, Astrid Johanne Meyer, Lorentz Petter Lossius, Kristian Etienne Einarsrud

Abstract Alumina, alongside with electricity and carbon, is the raw material used for production of aluminium in the Hall-Héroult process. An efficient dissolution process is important to acquire stable conditions for the cell, resulting in lower energy consumption. Under certain conditions, the alumina will not dissolve upon addition but remains afloat on the bath surface as a so called raft. The conditions under which the rafts form are still not fully understood, although it is likely that their behaviour is influenced by operational conditions which in turn depend upon bath and alumina properties. In order to obtain more knowledge on the conditions for raft formation, an industrial measurement campaign was performed at Alcoa Mosjøen in which raft behaviour was recorded alongside collection of bath and alumina samples as well as the rafts themselves. The current paper describes the procedure utilized for data collection together with an analysis of bath and alumina properties, aiming to correlate these with raft flotation times. Raft floating times were found to vary between 5 and 140 seconds during normal operating conditions.

Key words: Alumina feeding · Agglomeration · Rafts · Industrial sampling

Sindre Engzelius Gylver
Norwegian University of Science and Technology (NTNU), Department of Materials Science and Engineering, Trondheim, Norway, e-mail: sindre.e.gylver@ntnu.no

Nina Helene Omdahl
Alcoa, Mosjøen, Norway, e-mail: Nina.Omdahl@alcoa.com

Ann Kristin Prytz
Hydro Aluminum, Porsgrunn, Norway e-mail: ann.kristin.prytz@hydro.com

Astrid Johanne Meyer
Hydro Aluminum, Porsgrunn, Norway, e-mail: astrid.johanne.meyer@hydro.com

Lorentz Petter Lossius
Hydro Aluminum, Årdal, Norway e-mail: lorentz.petter.lossius@hydro.com

Kristian Etienne Einarsrud
Norwegian University of Science and Technology (NTNU), Department of Materials Science and Engineering, Trondheim, Norway, e-mail: kristian.e.einarsrud@ntnu.no

1 Introduction

Dissolution and distribution of alumina is a complex process involving simultaneous transfer of heat and mass as well as phase dynamics. Despite considerable efforts over the last decades, [1]-[9], the origin and consequence of certain phenomena remains unclear, particularly in an industrial setting. As previously pointed out by several authors, cf. [1] and [2], the dissolution and distribution of alumina is crucial for stable operations, even more so as the available bath volume is decreasing due to increasing anode size and amperage, in order to increase the overall efficiency of the process.

As pointed out in the recent review by Lavoie et al. [2], successful operations rely upon additional features in addition to dissolution, namely delivery (i.e. feeding), dispersion and distribution. Alumina feeding is typically performed using point feeders, in which a dose of 0.5-2 kg of alumina is fed at regular intervals of 1-3 minutes, depending upon cell size and number of feeders. Owing to the large temperature difference between the dose and bath - typically operating close to liquidus - bath will freeze onto the alumina particles and agglomerate, forming a so called raft consisting of partially dissolved alumina particles and frozen bath.

Besides operational conditions such as feeding rate and bath flow, material properties of the alumina (for instance specific surface area (BET), particle size distributions (PSD) and α-phase content), moisture and volatiles (determined by MOI and LOI) and bath conditions (AlF_3 and superheat) are all known to influence the overall dissolution rate [2, 7, 8]. As indicated by Lavoie et al., [2], most of the parameters influencing dissolution have been studied in controlled lab scale experiments, such as the recent experiments by Kazsas et al. [4], in which 0.1-2 g of alumina was added to a crucible containing molten bath. The spreading and shape of the raft as well as bath infiltration and raft disintegration was recorded. Kazsas et al. [4] note that the spreading of alumina was hindered by the size of the crucible. The spreading was also found to depend on superheat, where higher superheat resulted in larger rafts, while at the same time disintegrating at a higher rate. The observations are consistent with those presented in [2], however, as pointed out by the authors, the doses used are considerably smaller than those encountered industrially, potentially influencing the results.

Data on industrial rafts is scarce. Walker [9] observed feeding in an industrial cell and described a coherent floating island, which unlike crust was described as having a viscous and mushy consistency. Rafts are also described by Dando et al. [10] in experiments where smelter grade alumina (SGA) was added to a industrial cell and rafts induced, aiming to describe the interplay between HF evolution, raft formation and dissolution, concluding that raft formation promotes slow dissolution.

In order to obtain more knowledge on the conditions for raft formation, an industrial measurement campaign was performed at Alcoa Mosjøen in which raft behaviour was recorded alongside collection of bath and alumina samples as well as the rafts themselves. The current paper describes the procedure utilized for raft collection together with an analysis of bath and alumina properties, aiming to correlate

these with raft floating times - i.e. how long the raft remained afloat prior to disintegration. An analysis of raft composition and microstructure can be found in [11].

2 Experimental procedure

Two experimental campaigns were performed in July-August 2017 at Alcoa Mosjøen. In the first, the time which alumina remained floating on the bath surface was observed and registered manually, while bath properties were determined by means of a STARprobe^{TM} [12]. The bath height was measured manually and anode age was determined based on the anode changing cycle.

The second set of experiments followed a more extensive approach in which primary and secondary alumina samples were collected prior (primary) and during (secondary) experiments, alongside with bath samples taken before, between and after the collection of rafts. For each experiment, two rafts from two trailing feeding events were collected from the tap position of the cell by means of perforated skimming ladles with diameter 21-23 cm. The tap hole was extended when necessary in order to access the rafts and to ensure good conditions for visual observations. In order to have sufficient space for the ladle, cells with anodes older than 15 days on each side at the tap position were selected. Video recordings were performed using a SONY DSC-H4000 with a polarization filter, as well as STARprobe^{TM} measurements. Prior to sampling of rafts, the ladle was heated by keeping it close to the bath surface for 2 minutes. The rafts were first cooled down on the skimming ladle before being removed and stored in vacuumed bags for further analysis, cf. [11].

For each of the campaigns, samples were collected from different pots.

2.1 Bath analysis procedure

The samples of frozen bath were analyzed at Hydro Aluminium, Primary Metal, Technology. Sample preparation included crushing to a certain fineness, splitting and milling. The milled material was analyzed for oxygen by Leco-O combustion analysis and chemical composition of phases using x-ray diffraction (XRD). The quantitative determination was by full profile Rietveld refinement using a phase filter designed for regular bath with different aluminas and graphitic carbon dust. The principles of using phase filters is described in [13]. The bath acidity was computed from the bath composition. Carbon was set at 0.1wt% and trace impurities at 0.4wt%.

From experience, regarding detection limits, an XRD phase concentration level below 0.5wt% is uncertain; for cubic forms this limit is 0.3wt%. At such low concentrations, the phase should be confirmed by visual inspection of the diffractogram.

2.2 Alumina analysis procedure

The particle size distribution has been determined by laser diffraction using Mie model of light scattering by particles. Measurements have been performed with a Coulter LS200 instrument.

The surface area has been determined by both the Brunauer-Emmet-Teller method (BET) and the Barret-Joyner-Halanda method (BJH) by the use of a Micromeritics Tristar 3000 instrument. The samples (0.5-1 g) were evacuated for 2 hours at 150°C. The BET method was used for surface area determination according to standard method within the alumina industry (ISO 8008). The BJH method was used for the pore area evaluations, where the surface area above 3 nm is summarized based on the findings of McIntosh et al. [14], suggesting that pores smaller than 3 nm will be blocked and not contribute in the scrubbing of HF. BJH$>$3 nm thus indicates the available surface area.

MOI (20-300°C) and LOI (300-1000° C) levels have been determined by gravimetry in a furnace according to ISO 806. In addition, a modified method with the temperature range 20-160°C and 160-300°C, which separates contributions from adsorbed moisture and any Gibbsite present in the material was performed. LOI (300-1000°C) has only been measured for primary alumina. The residual hydroxyl content is not expected to be altered significantly during dry scrubbing and the analyses performed for primary alumina are thus considered relevant for the corresponding secondary alumina as well.

The fluoride content has been determined by use of Nuclear magnetic resonance (NMR) and measurements have been performed with a tabletop NMR system (MQC) from Oxford Instruments.

In addition, phase analysis was performed by powder-diffraction. Sample preparation was by milling and the quantitative determination was by full profile Rietveld refinement, including several modifications of alumina, including a near-amorphous Short Range Order (SRO) for of theta alumina. In addition to the alumina forms, secondary alumina will have some adsorbed moisture, fluorides and sulfur-containing species; with XRD, only solidus surface species were modelled, including $NaAlF_4$, AlF_3 and $Na_4Ca_4Al_7F_{33}$.

3 Results

3.1 First campaign

During the first campaign, a total of 13 experiments were made, summarized in table 1. Plots showing selected parameters are shown in figure 1. The floating time, t_f, i.e. the time the raft remains afloat after feeding was found to vary considerably - from immediate sinking to remaining afloat until the subsequent feeding.

Table 1 Summary of data from the first set of experiments and correlation coefficient to floating time - based on a 90% confidence interval. N/A is used where no statistically significant correlation was found. The raft floating time (t_f), bath height (h_{bath}) and anode age A_a were determined manually, while bath temperature (T_b), bath superheat (T_s), excess AlF_3 ($xsAlF_3$) and alumina concentrations (Al_2O_3) was determined using STARprobe^{TM}.

	t_f (s)	$xsAlF_3$ (wt%)	T_b (°C)	T_s (°C)	Al_2O_3 (wt%)	h_b (cm)	A_a (days)
Mean value	33	10.9	955.8	7.5	2.8	21	19
Std. dev.	23	1.5	11.5	3.5	0.6	2	4
Correlation to t_f	-	N/A	N/A	N/A	N/A	0.58	0.79

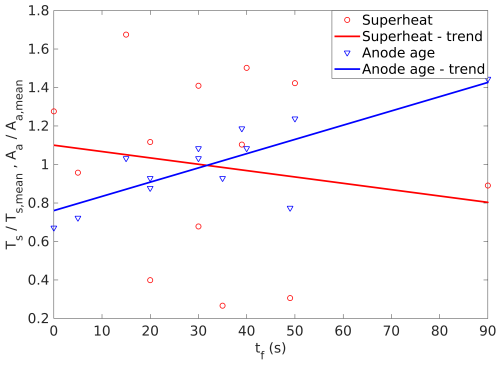

Fig. 1 Plots showing floating time t_f vs. bath superheat T_s and anode age A_a, both normalized to their mean values as of table 1.

3.2 Second campaign

During the second campaign, 6 experiments (12 raft samples) were made, in which 8 video recordings were successful. Primary alumina was collected prior to 4 of the experiments, while samples of bath and secondary alumina were collected alongside with STARprobe^{TM} measurements before, during and after each experiment. The typical behaviour for a raft on the bath surface is shown in figure 2. For this specific case, the crust was broken all the way between the feeding and tap hole for enhanced visualization. The alumina was found to spread on the open surface and was then gradually consumed from the sides, aided by gas bubbles escaping from the anodes, resulting in bath splashing on the floating raft. In the case shown in figure 2, the raft was completely dispersed before the next addition.

An example of a raft collected using the skimming ladle is shown in figure 3. There was a layer of pure oxide on the top, and then a mix between oxide and frozen bath, as indicated in figure 3(a) and (b). Further down, the raft seems to consist of multiple layers of frozen bath. It should be noted that it was not possible to recover the entire raft with the method described in the current work. Loose alumina, not infiltrated by bath, was for instance blown away while extracting the ladle. In some cases, the raft broke into several pieces upon removal, thus losing some parts of the raft.

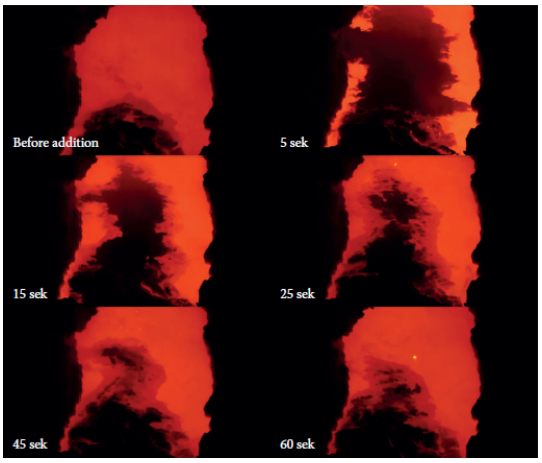

Fig. 2 Sample images from video recording where the crust has been broken between the feeding and tap hole for enhanced visualization. The dark area is floating undissolved alumina - e.g. a raft. The time is set relative to a single feeding event.

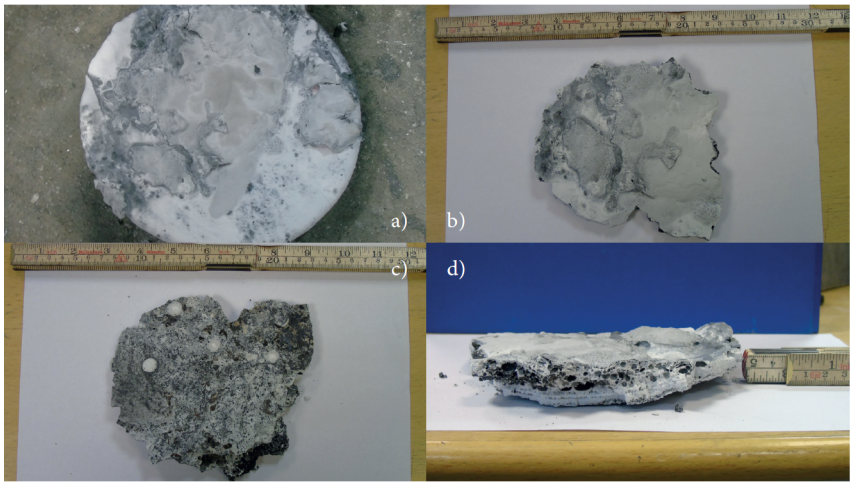

Fig. 3 Sample images of a raft, showing a) raft on the skimming ladle, b) seen from above (after removal from ladle), c) from underneath, d) from the side.

Results of the analysis for secondary alumina are shown in table 2, along with LOI 300-1000 values obtained for primary alumina. Corresponding results for the bath analysis is shown in table 3. Results shown in these tables are average values (were applicable) for each of the experiments. Selected parameters are plotted in figures 4 and 5 for reference.

Table 2 Summary of secondary alumina properties and LOI 300-1000 for primary alumina from the second campaign and correlation coefficient to floating time - based on a 90% confidence interval. N/A is used where no statistically significant correlation was found. The raft floating time (t_f) was determined by analyzing video footage, while alumina properties were determined following procedures described in section 2.2. Fluoride (F) represents the sum of fluoride solidus in secondary alumina.

Exp.	t_f	PSD				BET	BJH
		+150μm	+75μm	-45μm	-20μm		(>3nm)
(#)	(s)	(%)	(%)	(%)	(%)	(m^2/g)	(m^2/g)
1	135	5.6	70.9	7.9	2.0	64.1	71.3
2	70	6.1	65.5	9.8	2.2	71.5	76.9
3	40	5.2	70.8	8.0	2.1	67.0	74.8
4	75	5.2	68.3	8.6	2.0	70.2	75.3
5	-	5.3	65.1	11.1	2.8	70.6	78.1
6	70	5.3	69.7	9.4	2.5	69.0	74.3
Mean value	78	5.5	68.4	9.1	2.3	68.7	75.1
Std. dev.	35	0.4	2.6	1.2	0.3	2.8	2.3
Correl. to t_f	-	N/A	N/A	N/A	N/A	N/A	N/A

Exp.	MOI/LOI		Phases		F	LOI (primary)
	20-160	160-300	Alpha	Gibbsite		300-1000
(#)	(%)	(%)	(%)	(%)	(%)	(%)
1	1.37	0.58	1.3	0.5	8.3	0.82
2	1.16	0.66	3.0	0.5	3.5	0.85
3	2.39	0.82	1.3	0.3	3.0	-
4	1.24	0.69	1.3	0.5	3.0	0.84
5	1.01	0.73	1.3	0.5	3.0	0.83
6	1.66	0.71	1.5	0.5	3.0	-
Mean value	1.47	0.70	1.6	0.5	4.0	0.84
Std. dev.	0.50	0.08	0.7	0.1	2.1	0.01
Correl. to t_f	N/A	-0.92	N/A	N/A	0.92	N/A

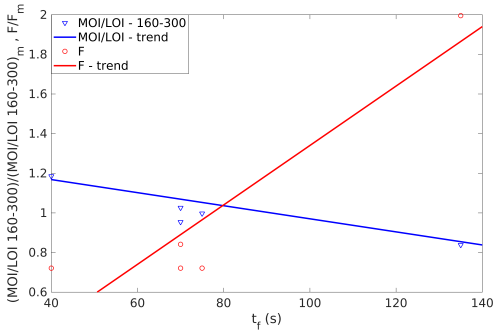

Fig. 4 Plots showing floating time t_f vs. MOI/LOI 160-300 and F, both normalized to their mean values as of table 2.

Table 3 Summary of bath properties from the second campaign and correlation coefficient to floating time - based on a 90% confidence interval. N/A is used where no statistically significant correlation was found. The raft floating time (t_f) was determined by analyzing video footage, while bath properties were determined following procedures described in section 2.1 or STARprobe^{TM} (SP).

Exp.	t_f	Cryolite XRD	Chiolite XRD	α-$NaCaAlF_6$ XRD	α-$Na_2Ca_3Al_2F_{14}$ XRD	Al_2O_3 XRD	Al_2O_3 LECO	Al_2O_3 SP
(#)	(s)	(wt%)	(wt%)	(wt%)	(wt%)	(wt%)	(wt%)	(wt%)
1	135	54.5	32.5	2.7	7.0	2.8	2.88	2.6
2	70	39.2	48.0	1.9	8.1	2.5	2.46	3.5
3	40	34.3	52.5	2.1	7.7	2.8	2.70	3.7
4	75	46.6	40.5	2.7	6.7	2.9	2.79	2.2
5	-	51.5	34.8	2.8	7.0	3.5	2.06	2.9
6	70	36.7	50.4	2.3	7.8	2.4	2.38	3.8
Mean value	78	43.8	43.1	2.4	7.4	2.8	2.55	3.1
Std. dev.	35	8.3	8.4	0.4	0.5	0.4	0.30	0.7
Correl. to t_f	-	0.92	-0.92	N/A	N/A	N/A	N/A	N/A

Exp.	$xsAlF_3$ XRD	$xsAlF_3$ SP	T_b SP	T_s SP	h_b	A_a
(#)	(wt%)	(wt%)	(°C)	(°C)	(cm)	(days)
1	10.2	9.6	966.6	6.3	21	27
2	14.0	12.4	949.0	8.7	21	22
3	15.1	14.5	941.8	11.1	20	15
4	12.1	12.8	953.5	4.5	24	14
5	10.8	10.7	955.5	3.4	-	-
6	14.6	12.7	946.1	9.6	21	21
Mean value	12.8	12.1	952.1	7.2	21	20
Std. dev.	2.1	1.7	8.7	3.0	2	5
Correl to t_f	-0.91	-0.99	0.97	N/A	N/A	0.78

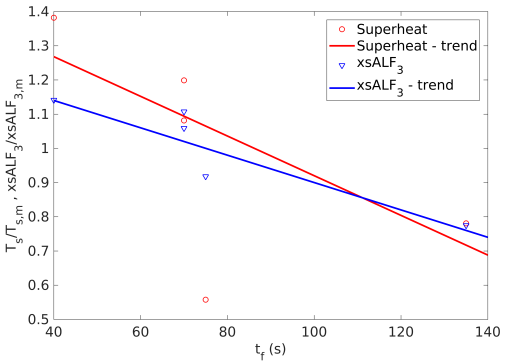

Fig. 5 Plots showing floating time t_f vs. bath superheat T_s and excess AlF_3, both normalized to their mean values as of table 3.

4 Discussion

As seen from tables 1-3, the observed floating time of the rafts varies from 5 to 140 seconds during normal operating conditions. For the first set of experiments, shown in table 1, no significant correlations are seen between floating times and the measured bath properties.

As seen from the data shown in figure 1, the spread in measured superheat is considerable, making the proposed trend line indicative at best. For the second set of experiments, cf. table 3, the same tendency is observed for superheat, although again without statistical significance. As pointed out by Lavoie et al. [2], low superheat has been found to strongly reduce the initial dissolution rate in laboratory experiments. The lower dissolution rate can be explained by increased bath freezing on the agglomerate, which also will result in a more rigid raft, less prone to disintegration and thus longer floating times - provided that the density of the raft is sufficiently low to keep it afloat - cf. [11].

The superheat did not have a noticeable influence upon the spreading of the alumina on the bath surface in the current experiments; the alumina would spread across most of the available bath area (cf. figure 2) in all of the cases considered. It should be noted that the available bath surface is greater in the current experiments than during operations, as the crust was broken in order to realize observations.

Although no significant influence of superheat was found, the temperature it self appears to be of importance, cf. table 3 - higher temperatures resulting in greater floating times. The bath temperature, while operating close to the liquidus, is inherently linked to the bath composition e.g. excess fluoride and cryolite to chiolite ratio, cf. for instance chapter 2 in Grjotheim et al. [16].

Considering the bath ratio, i.e. the weight ratio of NaF to AlF_3, the data in the second set of experiments indicate that lower bath ratios (i.e. more acid bath) yield lower floating times - consistently with temperatures. Conversely, lab scale measurements [17] have shown that lower bath ratios increase the dissolution time [2]. It should however be noted that this needs not be a contradiction as dissolution and floating times not necessarily are equivalent - as agglomerates very well may sink without dissolving, forming muck on the cathode. No significant correlation is found between bath ratio and floating times in the first set of experiments (table 1).

No definite conclusions can be drawn from the alumina concentrations. As seen from table 3, XRD and LECO data agree well, while STARprobe^{TM} measurements apparently give a larger variation. This discrepancy may be a result of differences in sampling positions and times for the measurements. There is a lack of agreement upon the influence of alumina concentrations upon dissolution times in the literature as well, provided that concentrations are below saturation, as is the case currently.

Several features of the alumina itself are expected to influence the feeding process and dissolution time, in particular the particle size (PSD) and phase distributions and effervescence through evolution of gaseous species, i.e. HF and water vapour. The data presented in table 2 is inconclusive regarding the influence of the PSD and phases, while increased moisture content is related to decreased floating times (MOI/LOI 160-300 data); most likely due to gas evolution within the raft as

it is heated, potentially breaking it into pieces which are more easily dispersed. The fluoride content also appears to be an important factor. As indicated by Haverkamp et al. [15], in relation to alumina dissolution, fluoride itself does not influence dissolution rate, but is suggested to improve water adsorption in the scrubbing process. The fluoride and moisture content should thus not be considered as fully independent parameters in the current setting.

A large correlation is found with cell conditions (i.e. anode age) to floating times - greater anode age apparently leading to longer floating times. As seen in figure 2, the raft disintegrates from the sides, partially due to bubble induced agitation of the bath surface. The departure rate of anodic gas bubbles increase with increasing anode age, cf. [18, 19], as slots become less important. At the same time, the amount of gas produced will be essentially unchanged, meaning that older anodes will produce smaller bubbles than younger anodes, albeit at a higher rate, thus changing bath circulation and turbulence profiles.

The observations related to temperature and excess fluoride may be linked to cell conditions as well, as the anode cathode distance (ACD) can be adjusted in order to compensate for low temperatures and high fluoride levels. These adjustments can in turn alter the flow conditions, which ultimately influence as raft floating time, as indicated above.

5 Conclusions

Despite the uncertainties and imperfections in the proposed method, raft samples have been successfully collected together with relevant process parameters, providing new data and insight on the complex dynamics of alumina feeding.

During normal operating conditions, rafts were found to remain afloat on the bath surface between 5 and 140 seconds, by means of direct observations and video recordings. Although there is a considerable variation in the data, resulting in statistically insignificant correlation coefficients for many parameters, a few stand out as important. The anode age and thus available bath surface and circulation appear to have a strong influence on the floating time. Although superheat, linked to the freezing and melting of bath on the agglomerate, was expected to influence the behaviour of the rafts, no definite conclusions could be drawn from the current data. Bath temperature and composition were however shown to have a statistically significant correlation to the floating time. Regarding secondary alumina properties, moisture and fluoride content appear to have a significant influence upon the floating time, although possibly not independently of each other.

The influence of alumina concentrations on the floating time is inconclusive and results from bath samples and STARprobe^{TM} data suggest somewhat different values. However, since the influence of alumina dissolved in the bath is expected to be small on floating times, this discrepancy is not deemed critical. Data for excess fluoride appears to be fairly consistent, with a statistically significant correla-

tion to floating time, indicating that future data may be conveniently collected by STARprobe^{TM} alone.

Factors related directly to the feeding procedure, i.e. feeding rates, heights and masses have not been considered currently, but will be in future work.

Acknowledgements This work is funded by SFI Metal Production, Centre for Research-based Innovation, 237738. Financial support from the Research Council of Norway and the partners of SFI Metal Production is gratefully acknowledged.

References

1. Dassylva-Raymond, V., Kiss, L.I., Poncsak, S., Chartrand, P., Bilodeau, J.-F., Guerard, S.: Modeling the behaviour of alumina agglomerate in the Hall-Héroult process. In: Grandfield, J. (ed.) Light Metals 2014, pp. 603-608, Wiley, Hoboken (2014)
2. Lavoie, P., Taylor, M. P., Metson, J.B.: A Review of Alumina Feeding and Dissolution Factors in Aluminium Reduction Cells. Met. Mat. Trans. B **47**, pp. 2690-2696 (2016)
3. Thonstad, J., Solheim, A., Rolseth, S., Skar, O.: The Dissolution of Alumina in Cryolite melts. In: Bearne, G., Dupuis, M., Tarcy, G. (eds.): Essential Readings in Light Metals Volume 2, pp. 105-111, Springer, Cham (2016)
4. Kaszas, C., Kiss, L., Poncsak, S., Guerard, S., Bilodeau, J.F.: Spreading of Alumina and Raft Formation on the Surface of Cryolitic Bath. In: Ratvik, A.P. (ed.) Light Metals 2017, pp. 473-478, Springer, Cham (2017)
5. Østbø, N.P.: Evolution of Alpha Phase Alumina in Agglomerates upon Addition to Cryolitic Melts. Ph.D. Thesis 50, Norwegian University of Science and Technology - NTNU, (2002)
6. Haverkamp, R.G., Welch, B.J.: Modelling the dissolution of alumina powder in cryolite. Chemical Engineering and Processing **37**,pp. 177-187 (1998)
7. Kaszas, C., Kiss, L., Guerard, S., Bilodeau, J.F:. Behavior of powders on the surface of a liquid. In: Hyland, M. (ed.) Light Metals 2015, pp. 639-642. Wiley, Hoboken (2015)
8. Lindsay, S.J.: Key Physical Properties of Smelter Grade Alumina. In: Grandfield, J. (ed.) Light Metals 2014, pp. 597-601. Springer, Cham (2014)
9. Walker, D.I.: Alumina in aluminum smelting and its behaviour after addition to cryolite-based electrolytes. Phd Thesis, Univeristy of Toronto, Toronto (1993)
10. Dando, N., Wang, X., Sorensen, J., and Xu, W.:Impact of thermal pretreatment on alumina dissolution rate and HF evolution. In: Johnson, J.A. (ed.) Light Metals 2010, pp. 541-546, Wiley, Hoboken (2010)
11. Gylver, S.E., Omdahl, N.H., Rørvik, S., Hansen, I., Nautnes, A., Neverdal, S.N., Einarsrud, K.E.: The micro- and macrostructure of alumina rafts. In: Chesonis, C. (ed.) Light Metals 2019, Springer, Cham (2019)
12. Wang, X., Hosler, B., Tarcy, G.: Alcoa STARprobe^{TM}. In: Lindsay, S. (ed.) Light Metals 2011, pp. 483-489, Wiley, Hoboken (2011)
13. Simon, D. E., Morton, R. W.: Rietveld Analysis For Industrial Applications. Denver X-ray Conference Workshop, Denver (2001)
14. McIntosh, G. J., Metson, J. B., Niesenhaus, T., Reek, T., Perander, L.: Smelter Fluoride Balances: The Interplay Between Alumina Phases, Pore Size Distributions, and the Impacts of Weather. JOM **66**, pp. 2272-2281 (2014)
15. Haverkamp, R., Welch, B., Metson, J.: The influence of fluorination on the dissolution rate of alumina in smelter electrolyte. In: Mannweiler, U. (ed.) Light Metals 1994, pp. 365-370, TMS, Warrendale (1994)
16. Grjotheim, K., Krohn, C., Malinovsky, M., Matiasovsky, K., Thonstad, J.: Aluminium Electrolysis, Fundamentals of the Hall-Héroult process, 2nd Edition. Alumimium Verlag, Dusseldorf (1982)

17. Kuschel, G.I., Welch, B.J.: Further studies of alumina dissolution under conditions similar to cell operations. In: Rooy, E. (ed.) Light Metals 1991, pp. 112-118, TMS, Warrendale (1991)
18. Einarsrud, K.E.: A treatise on interpolar transport phenomena. Ph.D. Thesis 201, Norwegian University of Science and Technology - NTNU, (2012)
19. Keniry, J.T., Barber, G.C., Taylor, M.P., Welch, B.J.: Digital processing of anode current signals: An opportunity for improved cell diagnosis and control. In: Anjier J.L. (ed.) Light Metals 2001, pp. 1225-1232, Wiley, Hoboken (2001)